Eur. Phys. J. A **10**, 49–56 (2001)

THE EUROPEAN PHYSICAL JOURNAL A

© Società Italiana di Fisica
Springer-Verlag 2001

One-nucleon removal cross-sections for ^{17,19}C and ^{8,10}B

D. Cortina-Gil[1,a,b], T. Baumann[1,c], H. Geissel[1], H. Lenske[2], K. Sümmerer[1], L. Axelsson[3], U. Bergmann[4], M.J.G. Borge[5], L.M. Fraile[5], M. Hellström[1], M. Ivanov[6,d], N. Iwasa[7], R. Janik[6], B. Jonson[3], K. Markenroth[3], G. Münzenberg[1], F. Nickel[1], T. Nilsson[3], A. Ozawa[7], K. Riisager[4], G. Schrieder[8], W. Schwab[1], H. Simon[8], C. Scheidenberger[1], B. Sitar[6], T. Suzuki[7], and M. Winkler[1]

[1] Gesellschaft für Schwerionenforschung, 64291 Darmstadt, Germany
[2] Institut für Theoretische Physik I, 35392 Giessen, Germany
[3] Fysiska Institutionen, Chalmers Tekniska Högskola, 412 96 Göteborg, Sweden
[4] Institut for Fysik og Astronomi, Aarhus Universitet, 8000 Aarhus C, Denmark
[5] Instituto de Estructura de la Materia, CSIC, 28006 Madrid, Spain
[6] Faculty of Mathematics and Physics, Comenius University, 84215 Bratislava, Slovakia
[7] RIKEN, 2-1 Hirosawa, Wako, Saitama 351-01, Japan
[8] Institut für Kernphysik, Technische Universität Darmstadt, 64289 Darmstadt, Germany

Received: 26 July 2000 / Revised version: 5 December 2000
Communicated by D. Guerreau

Abstract. One-neutron removal cross-sections (σ_{-1n}) of ^{17,19}C in various targets at about 900 MeV/nucleon, and one-proton removal cross-sections (σ_{-1p}) of ^{8,10}B at about 1400 MeV/nucleon were measured using the fragment separator FRS at GSI. A significant increase of σ_{-1n} for ^{19}C compared to its neighbors was observed. The same behavior was found for σ_{-1p} for the neutron-deficient nucleus ^{8}B compared to the stable isotope ^{10}B. These results support a one-neutron halo structure in ^{19}C and a one-proton halo in ^{8}B.

PACS. 25.60.Gc Breakup and momentum distributions – 27.20.+n Properties of specific nuclei $6 \leq A \leq 19$

1 Introduction

Studies of dripline nuclei have shown that a small separation energy of the last bound nucleon is a necessary but not sufficient condition for a halo structure. In this sense, the small proton and neutron separation energies in ^{8}B ($S_p = 137 \pm 1$ keV [1]) and ^{19}C ($S_n = 162 \pm 112$ keV [1], $S_n = 240 \pm 100$ keV [2], or $S_n = 530 \pm 130$ keV [3]) provide important but incomplete evidence for halo structures. A confirmation can only be achieved by studies of additional observables which provide specific information on the wave functions involved. Measurements of reaction and interaction cross-sections and longitudinal momentum distributions are established tools for such studies. Reaction and interaction cross-sections (σ_R, σ_I) for ^{8}B on different targets have been measured at a variety of incident energies during the last years [4–12]. A σ_R slightly larger than that of the neighboring stable nuclei ^{12}C and ^{14}N was observed for ^{8}B on a Si target at intermediate energies between 20 and 60 MeV/nucleon [6]. This fact was interpreted in terms of a proton-halo in ^{8}B. However, σ_I measurements at relativistic energies seem to be compatible with a normal size of ^{8}B [10,11]. In the carbon case, almost the full range of particle stable neutron-rich isotopes has been explored. The unusual properties of ^{19}C were emphasized by the sudden increase of its interaction cross-section measured at relativistic energies at GSI [13].

Valuable information on wave functions is obtained from measurement of longitudinal momentum distributions. During the last years, ^{8}B [5,11,14] and ^{19}C [2,15, 16] have been investigated at MSU, GANIL, and GSI. The exceptionally narrow momentum distributions of the fragments from ^{8}B and ^{19}C single-nucleon removal reactions were interpreted as hints of one-nucleon halo structures. Recent FRS measurements of momentum distributions of ^{7}Be and ^{16,18}C fragments from breakup reactions of ^{8}B [17] and ^{17,19}C [18], respectively, point to the same conclusion.

In this paper we investigate one-nucleon removal cross-sections (σ_{-1N}, here N stands for n or p) as additional observables for halo studies. Removal cross-sections and momentum distributions are determined by the same processes. While the latter are differential observables, the removal cross-sections provide a measure of the total

[a] *Present address:* Universidad de Santiago de Compostela, Spain
[b] e-mail: d.cortina@usc.es, d.cortina@gsi.de
[c] *Present address:* NSCL, Michigan State University, East Lansing, USA
[d] *Present address:* GSI Darmstadt, Germany

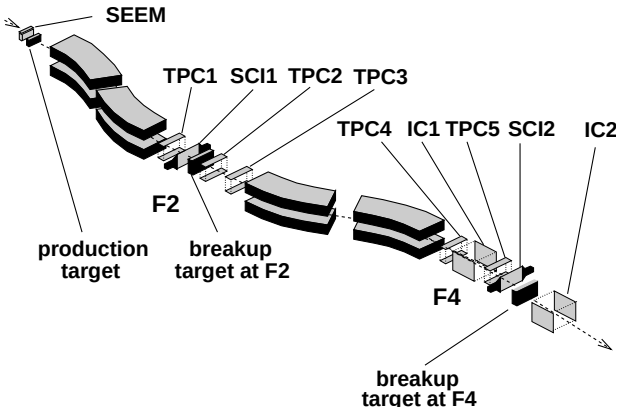

Fig. 1. Experimental setup for longitudinal momentum measurements with the FRS operated in energy-loss mode. SEEM is a secondary-electron emission monitor, TPC are time projection chambers, SCI are plastic scintillators, and IC are ionization chambers.

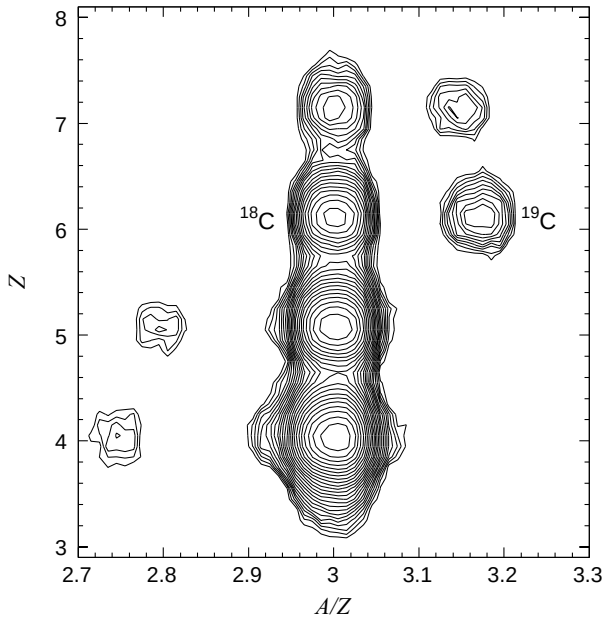

Fig. 2. Fragment-identification plot at the final focus of the FRS. An ionization chamber (IC1) was used for the identification of Z. A/Z was calculated from time of flight and magnetic rigidity measured in the second half of the FRS as described in the text. The contours represent a logarithmic scale.

breakup yield into this channel, thus representing a complementary source for structure information. One-nucleon removal cross-sections of secondary ^{8}B and ^{17,19}C beams were measured and the results compared with results for tightly bound reference systems from the same isotopic chain, namely ^{12}C measured earlier by Olson *et al.* [19], and ^{10}B measured in the same experiment as ^{8}B.

2 Experimental setup and results

A schematic view of the experimental setup is shown in fig. 1. To produce secondary beams of radioactive nuclei, primary beams of stable isotopes from the heavy-ion synchrotron (SIS) at GSI were fragmented in a thick Be target placed at the entrance of the FRS [20]. The first half of the FRS was set to transport the selected secondary beam to the intermediate focal plane F2, where a breakup target was installed.

The second half of the FRS was set to the magnetic rigidity of the fragments arising from one-nucleon removal reactions of the selected secondary beams. Particles arriving at the final focus F4 were identified by measuring the time-of-flight between the scintillators SCI1 and SCI2, by determining the magnetic rigidity ($B\rho$) from position measurements in position-sensitive time projection chambers (TPC), and by a coincident energy-deposition measurement in an ionization chamber (IC1). The different isotopes were well separated in a Z *versus* A/Z plot as is shown in fig. 2.

The fragment separator allows a selection according to the mass-to-charge ratio of the particles impinging onto the F2 breakup target (see fig. 1). In front of the F2 breakup target only a charge identification of the secondary projectiles was possible with the present experimental setup (SCI1). The number of particles of a certain isotope arriving at the F2 breakup target was therefore calibrated in a different setting of the FRS. In this setting, the F2 breakup target was removed and the beam arriving at the mid-plane F2 was completely transmitted to the final focal plane F4, where the particles could be fully identified with respect to A and Z. With this setting, the composition of the secondary beam was measured. Knowing the composition of the particle beam at the mid-plane F2 and the ratio of the selected projectile to the primary beam intensity measured with a secondary-electron emission monitor (SEEM), the number of projectiles impinging onto the F2 breakup target could be deduced for any measurement, provided that the setting of the first half of the FRS was identical.

With the F2 breakup target inserted, the second half of the FRS was set to select the one-nucleon removal product, which was fully identified with respect to A and Z at the final focus F4. From the ratio of the number of projectiles impinging onto the F2 breakup target and the number of fragments arising from the one-nucleon removal channel — corrected for acquisition dead time, secondary reactions, and transmission losses — the one-nucleon removal cross-sections were deduced.

2.1 The ^{8}B case

The boron isotopes ^{8}B and ^{10}B were produced by fragmentation of a ^{12}C primary beam of 1.5 GeV/nucleon in a ^{9}Be target of 8.0 g/cm^2 thickness. The primary beam intensity was approximately $1.5 \cdot 10^8$ particles per spill at 1/8 s repetition rate.

The first half of the FRS was set to the $B\rho$ value of ^{8}B (^{10}B) fragments. Behind the F2 breakup target the magnetic fields were set to select the 1p-removal product ^{7}Be (^{9}Be), which was identified with respect to A and Z

Table 1. Experimental one-proton removal cross-sections for ^{8,10}B on different targets. The values in column 2 correspond to mid-target energies. This table also lists the individual cross-sections for ^{8}B obtained with the F2 and F4 breakup targets and their weighted average.

	Energy (MeV/u)	Target		σ_{-1p} (mb)	σ_{-1p} (mb)
^{8}B	1440	C	F2	85 ± 14	98 ± 6
	1440	C	F4	100 ± 5	
	1471	C			94 ± 4[a]
	1440	$(CH_2)_n$			103 ± 17
	1440	Pb			687 ± 117
^{10}B	1450	C			17 ± 2

[a] From ref. [11].

at F4. The presence of ^{7}Be (^{9}Be) contaminants at F4 not stemming from the 1p-removal channel was investigated in detail. There are considerable contributions of ^{7}Be (^{9}Be) to the secondary beam arriving at the breakup target at F2, but these nuclei were not transmitted to the final focal plane due to the large change in $B\rho$ between the two magnetic stages of the FRS of more than 5%, which is well outside the FRS acceptance of $\Delta B\rho \approx 1\%$. Contaminations from projectiles other than ^{8}B (^{10}B), but reacting to form ^{7}Be (^{9}Be) fragments in the target, were discriminated by setting a gate onto the measured proton number Z in front of the F2 breakup target. The transmission of the fragments through the FRS was calculated with the ion-optical ray-tracing code MOCADI [21]. The widths of the simulated fragment momentum distributions were adjusted to the results of our momentum measurements [17].

The results obtained for ^{8}B on different targets and for ^{10}B on a C target are summarized in table 1. The errors assigned to the listed values are mainly due to the uncertainties in the calculation of transmission losses. For the ^{8}B case, the 1p-removal cross-section was independently deduced in a slightly different way in order to check the method of calculating the number of incoming ^{8}B projectiles. A second breakup target was installed at F4 between two ionization chambers (IC1 and IC2) for the measurement of charge-changing cross-sections (see fig. 1). For the particular case of ^{8}B, the 1p-removal reaction to ^{7}Be is the only possible exit channel for charge-changing reactions of ^{8}B to beryllium. Therefore, a charge measurement in IC2 of the products from the ^{8}B breakup is sufficient to select the 1p-removal channel and to measure its cross-section. In table 1, the result from this F4 measurement is compared with the one obtained using a reaction target at F2. The weighted average of these F2 and F4 cross-section measurements leads to a value of 98 ± 6 mb (see table 1, last column). The result of a previous measurement with the reaction target at F4 and a similar setup [11] is included in this table. The results of these three measurements are in perfect agreement.

The total interaction cross-section ($\sigma_{\rm I}$) for ^{8}B was also measured with the breakup target at the final focus F4.

Table 2. Experimental one-neutron removal cross-sections for ^{12,17,19}C on different targets. Beam energies in column 2 refer to mid-target energies. The value for ^{12}C was reported by Olson *et al.* [19].

	Energy (MeV/u)	Target	σ_{-1n} (mb)
^{12}C	1050	C	44.7 ± 2.8[a]
^{17}C	904	C	129 ± 22
^{19}C	910	C	233 ± 51
	910	Pb	1967 ± 334

[a] From ref. [19].

Since the only possible reaction channels for ^{8}B involve a change of charge, the total interaction cross-section could be measured in the same way as the 1p-removal cross-section, but counting the surviving ^{8}B nuclei instead of the reaction products. The value for $\sigma_{\rm I}(^{8}{\rm B})$ at 1440 MeV/nucleon that we obtained in this measurement is 831 ± 10 mb, in agreement with the value of 809 ± 11 mb obtained in a previous FRS experiment [11].

It should be noted that the uncertainties in the measurements with a reaction target at the final focus F4 are much smaller than in the cases where we used a reaction target at the mid-plane F2 because there are no transmission losses between the large size detectors IC1 and IC2 mounted directly in front of and behind the reaction target.

2.2 The ^{19}C case

For the measurements with carbon isotopes, SIS delivered an ^{40}Ar primary beam of 1 GeV/nucleon with an intensity of approximately $8 \cdot 10^{9}$ particles per spill at 1/8 s repetition rate. For the production of the secondary beam, a ^{9}Be target of 6.33 g/cm^2 thickness was placed at the entrance of the FRS.

Two secondary carbon beams, ^{19}C and ^{17}C, were studied. In these cases the reaction products of the one-neutron removal were ^{18}C and ^{16}C, respectively. Contamination by ^{18}C (^{16}C) nuclei produced in the production target could be ruled out as in the case of ^{8}B. Contamination from other reactions populating the final ^{18}C (^{16}C) channel was measured by identifiying the proton number in front of the breakup target at F2. The remaining contamination was less than 2% and was taken into account in the error assigned to the results. Transmission losses were corrected for in the same way as described for the boron isotopes.

The one-neutron removal cross-sections with their corresponding errors are summarized in table 2. The main source for the experimental errors lies in the determination of the transmission losses in the FRS. The value for the one-neutron removal cross-section of ^{12}C reported by Olson *et al.* [19] is shown here for comparison with the neutron rich nuclei ^{17,19}C.

Table 3. Compilation of BEVALAC data for experimental one-neutron removal (σ_{-1n}) and one-proton removal (σ_{-1p}) cross-sections for different stable beams [19].

	Energy (MeV/u)	Target	σ_{-1n} (mb)	σ_{-1p} (mb)
^{12}C	1050	C	44.7 ± 2.8	48.6 ± 2.4
	2100	C	46.5 ± 2.3	53.8 ± 2.7
^{16}O	2100	C	42.9 ± 2.3	54.2 ± 2.9

3 Discussion

With their low one-nucleon separation energies, ^{8}B and ^{19}C fulfill one of the conditions to be considered as one-proton or one-neutron halo nuclei. The strongest indication for the actual presence of such structures are the narrow momentum distributions observed in breakup reactions for both nuclei [2,5,11,14–18].

In earlier experiments we observed that the ^{8}B interaction cross-sections $\sigma_{\rm I}$ showed a strong energy dependence. These observations at low-energy measurements suggested the existence of a proton-halo in ^{8}B [4–10], but no clear signature of such a structure was seen at higher energies [11,12]. This fact indicates that reaction-dynamical effects are superimposed, thus inhibiting a direct access to the structure information.

Very likely, reaction cross-section measurements are rather insensitive to the structural details of halo states. By definition, they sum over all exit channels and, especially, over all orientations. The summation over all orientations causes a lack of selectivity on the *orbital* angular momentum and the projection quantum numbers of the removed nucleon.

This effect is absent for $\ell = 0$ halo states, *e.g.* in ^{11}Be [22,23], such that the interaction cross-sections $\sigma_{\rm I}$ provide an evidence of halo existence, but it contributes to ^{8}B measurements where $\ell = 1$. This indicates that in order to identify halo states, an observable of less integral character than $\sigma_{\rm R}$ or $\sigma_{\rm I}$ is required.

For that purpose, the nucleon-removal cross-sections σ_{-1N}, recording the breakup yield into a well-defined final channel, are suitable quantities. They carry much more specific information on the system properties than global quantities like $\sigma_{\rm R}$ and $\sigma_{\rm I}$.

3.1 Discussion of ^{8}B cross-sections

Our measurements can be compared with former BEVALAC (Lawrence Berkeley Laboratory) results for proton removal from stable nuclei [19], displayed in table 3. For carbon targets at incident energies of 1–2 GeV/nucleon, a value of $\sigma_{-1p} \approx 50$ mb is seen to be typical for one-proton removal from stable nuclei. For ^{8}B, the measured σ_{-1p} is larger by a factor of about 1.8.

The spin and parity of the ^{8}B ground state (2^{+}) is known experimentally. The simplest configuration for the ^{8}B ground state that one can imagine would be a $1p_{3/2}$ proton coupled to the ^{7}Be($3/2^{-}$) ground state. However, theoretical calculations using either a mean-field-plus-RPA approach or a cluster model [11,17,24] predict a more complicated structure. According to both of these calculations, the "simplest" configuration mentioned above amounts to about 70% of the ^{8}B wave function. In addition, admixtures of $1p_{1/2}$ and $1p_{3/2}$ proton states coupled to the first excited ^{7}Be state at 430 keV ($1/2^{-}$) contribute at the 15% level each. Both the mean-field-RPA and the cluster-model wave functions, show typical halo properties. In the mean-field approach [24], for example, the proper halo component covers about 25% of the total probability density.

When describing reaction dynamics in an eikonal approach, the RPA [24] wave function leads to a calculated value for σ_{-1p} of 104 mb, whereas the cluster model [17] yields 92–96 mb, both in good agreement with the experimental value listed in table 1. Since both theories also describe the measured momentum distributions quite well, the calculations give additional evidence for a halo in ^{8}B. However, theory also indicates that breakup reactions of proton halo systems are much stronger affected by reaction dynamics than those of neutron halo states. In ^{8}B this is mainly due to the fact that Coulomb and centrifugal potentials confine the wave function to the nuclear interior. As a consequence, the fraction of the wave function found outside the core region is suppressed compared to a neutron state of the same angular momentum. The strong influence of the Coulomb barrier is clearly demonstrated by replacing artificially the ^{8}B valence proton by a neutron in a $1p_{3/2}$ state of the same binding energy. Comparing the root-mean-square radii from the realistic proton and the illustrative neutron calculations, values of 4.95 fm and 5.66 fm, respectively, are found, although the asymptotic behaviour of both wave functions is governed by the same exponential decay constant which is determined by the small separation energy of 137 keV. This illustrative example shows that the important difference between proton and neutron halo states is the asymptotic normalization reflecting the (quantum mechanical) probability to find the particle at large distances from the core. Because breakup cross-sections scale roughly with the normalization constant of this asymptotic halo part of the wave function, the removal cross-section is reduced accordingly. Another consequence of the barrier effect is that proton breakup reactions become especially sensitive to penetrability and absorption effects in the in- and outgoing reaction channels and to final-state interactions of the knocked-out particle, see, *e.g.*, ref. [25].

For ^{10}B, an at first sight surprisingly small value of $\sigma_{-1p} = 17$ mb is measured as shown in table 1. This apparent suppression is related to the special properties of the ^{9}Be residual nucleus which does not have bound excited states. Consequently, there are less final states available after proton removal than for other stable nuclei. Considering that σ_{-1p} is an inclusive quantity including contributions from excited states in the target and, in particular, from all bound excited states in the outgoing projectile-

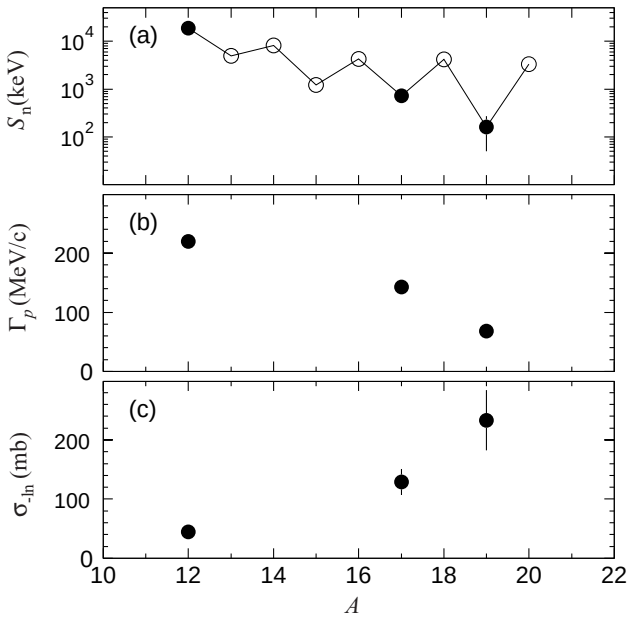

Fig. 3. Neutron separation energies, S_n (a), the measured widths, Γ_p (FWHM), of the longitudinal momentum distributions [18,26] (b), and the measured one-neutron removal cross-sections (c) for carbon isotopes impinging on carbon targets, plotted as a function of mass number A. Filled circles in (a) correspond to isotopes discussed in the present paper.

like fragment, the suppression can be understood, at least qualitatively.

3.2 Discussion of ^{19}C cross-sections

Since many more experimental data are available for the carbon isotopes than for the boron isotopes, we can display the systematics of some quantities relevant for the halo structure of these nuclei in fig. 3. The evolution of the one-neutron separation energy, S_n, with mass number is presented in fig. 3 (a) for different carbon isotopes [1]. For ^{19}C we observe a dramatic decrease of S_n, which is much larger than the systematic odd-even effect, even though the measured or derived values of S_n are inconsistent [1–3], leading to the larger error bar for ^{19}C. In fig. 3 (b) we plot the widths (FWHM) Γ_p of the longitudinal momentum distributions of the fragments after breakup reactions of ^{12}C, ^{17}C, and ^{19}C in carbon targets [18,26]. Finally, fig. 3 (c) displays the one-neutron removal cross-sections for the neutron-rich isotopes ^{17}C and ^{19}C, in comparison to the value for the stable ^{12}C reported by Olson *et al.* [19].

Measurements of σ_{-1n} for light stable nuclei at incident energies of 1–2 GeV/nucleon [19], summarized in table 3, show a value of $\approx$ 45 mb. Our cross-sections for ^{17,19}C exceed this reference value by factors of about 3 and 5, respectively. Even more relevant for halo studies is the strong increase from ^{17}C to ^{19}C. The increase in removal cross-section with increasing neutron excess by a factor of 2 nicely correlates with the decrease of the widths of the corresponding momentum distributions [18]. The results show that one-nucleon removal cross-sections, in combination with other information, give a more complete picture of dripline nuclei than reaction cross-sections or momentum distributions alone.

The theoretical picture of ^{19}C is less clear than for ^{8}B, mainly because neither the one-neutron separation energy (S_n) nor spin and parity (J^π) of the ^{19}C ground state are known precisely. Any theoretical prediction of either of these quantities must, therefore, be checked against complementary experimental observables.

Ridikas *et al.* [27] investigated the nuclear structure of ^{15,17,19}C in a particle-rotor coupling model assuming statically deformed ^{14,16,18}C core ground states. From their calculations they concluded that the ground state of ^{19}C should have a J^π of $3/2^+$ or $5/2^+$, based on the good agreement between the shapes of theoretical and experimental one-neutron removal momentum distributions measured at $E/A \approx 80$ MeV, which were the only available data at that time. However, this J^π assignment appears to be in strong conflict with $\sigma_{-1n} = 233\pm51$ mb presented in table 2. Ridikas *et al.* [27] obtained a σ_{-1n} for ^{19}C+Be of 63.8 mb for $J^\pi = 3/2^+$ and $S_n = 240$ keV which can be considered as an upper limit for the same datum measured at 1.4 GeV/nucleon.

Assuming instead a $J^\pi = 1/2^+$ ground state, the authors predict $\sigma_{-1n} = 144$ mb. This value is in better agreement with our experimental result for σ_{-1n} but leads to a too narrow ^{18}C momentum distribution, considerably underestimating the observed width [18]. However, uncertainties caused by the reaction mechanism might affect that conclusion. The authors also present a calculation made for a $J^\pi = 1/2^+$ ground state assuming $S_n = 500$ keV, but they could not reproduce the experimental one-neutron removal momentum distribution nor the corresponding cross-section.

The conclusions of the ^{19}C Coulomb dissociation experiment performed at RIKEN by Nakamura *et al.* [3] point to a $J^\pi = 1/2^+$ ^{19}C ground state. A separation energy of $S_n = 530 \pm 130$ keV was extracted from the breakup data.

A few-body theoretical description by Tostevin and Al-Khalili [28] yielded preference for a $J^\pi = 1/2^+$ ground state using the experimental interaction cross-section of ^{19}C measured by Ozawa *et al.* [13] and a separation energy of $S_n = 240$ keV. This work excludes the $J^\pi = 3/2^+$ and $J^\pi = 5/2^+$ ground states. However, these authors pointed out that the data could also be described with a ^{19}C ground state with the valence neutron in a pure $s_{1/2}$ state and $S_n = 500$ keV.

Recent results from MSU [29], including coincidence measurements of γ-rays emitted from the ^{18}C fragments, indicate a $1/2^+$ ground state for ^{19}C and support the larger separation energy found by Nakamura *et al.* [3].

We also find a $1/2^+$ ground state for ^{19}C in a many-body theoretical approach using Hartree-Fock theory and including dynamical core polarization (DCP) by quasiparticle RPA (QRPA) methods [24,30–32]. In this ap-

Table 4. Calculated ground-state spins, one-nucleon separation energies, ground-state spectroscopic factors, one-nucleon removal cross-sections, and widths of momentum distribution after one-nucleon removal derived from dynamical core-polarization calculations for the case of a carbon target. The dependence of the single-neutron removal cross-section (σ_{-1n}) and the width of the momentum distribution (Γ_p) on the neutron separation energy S_n in ^{19}C is shown in the table. Wave functions from core-polarization calculations were used in relativistic eikonal breakup calculations at $E/A = 910$ MeV/nucleon.

	J^π	S_N (keV)	$S(J^\pi$, g.s.)	σ_{-1N} (mb)	Γ_p (MeV/c)
^{8}B	2^+	130	0.69	104	75
^{11}Be	$1/2^+$	510	0.74	123	43
^{17}C	$5/2^+$	760	0.61	124	132
^{19}C		160		196	61
	$1/2^+$	263	0.41	192	69
		500		126	80

Table 5. Comparison between theoretical and experimental values for one-nucleon removal cross-sections and for widths of momentum distributions (values for Γ_p are FWHM). The experimental data on carbon targets are those presented in this paper and in refs. [17,26,18,19]. The theoretical quantities were obtained with core-polarized wave functions and eikonal reaction calculations. One-proton and one-neutron removal reactions are indicated by -1p and -1n, respectively.

		Energy (MeV/u)	σ_{-1N} (mb) theo.	σ_{-1N} (mb) exp.	Γ_p(MeV/c) theo.	Γ_p(MeV/c) exp.
^{8}B	-1p	1440	*104*	98 ± 6	*75*	91 ± 5^a
^{10}B	-1p	1450	*17*	17 ± 2	*145*	165 ± 8^b
^{12}C	-1p	1050	*49*	48.6 ± 2.4^c	*178*	
^{12}C	-1n	1050	*46*	44.7 ± 2.8^c	*182*	220 ± 12^b
^{17}C	-1n	904	*124*	129 ± 22	*132*	143 ± 5^d
^{19}C	-1n	910	*192*	233 ± 51	*69*	68 ± 3^d

[a] From ref. [17].
[b] From ref. [26].
[c] From ref. [19].
[d] From ref. [18].

proach, states in an odd-mass nucleus like ^{19}C are described as superpositions of static mean-field and core-excited configurations. The mean-field component of the full wave function accounts for the motion of the valence neutron with respect to the inert ^{18}C (0^+) core. Interactions between the core nucleons and the valence particle, that excite the core nucleus and rescatter the extra nucleon into other orbits, are taken into account by the core-polarization components. A similar approach using a particle-vibration model was applied in [33] to ^{11}Be. In ^{19}C, interactions with the ^{18}C(2^+_1,1.67 MeV) state are the most important ones by which the valence particle is rescattered into d-wave orbits. The DCP processes result in additional dynamical (*i.e.* energy- and state-dependent) polarization self-energies, which are especially important in the $2s_{1/2}$ channel. For $S_n = 260$ keV the reduced spectroscopic factors for the leading particle configuration ^{18}C(0^+, g.s.)$\otimes 2s_{1/2}$ and the next most important ^{18}C(2^+_1,1.67)$\otimes 1d_{5/2}$ configuration are 0.41 and 0.52, respectively [1]. The strong suppression of the single-particle mean-field component is a direct consequence of the softness of ^{18}C against small external perturbations by the valence neutron. DCP results for halo nuclei are summarized in table 4. The calculated results will be compared to experimental data below.

The DCP wave functions are used in reaction calculations describing the longitudinal momentum distributions and removal cross-sections in an eikonal distorted-wave approach. In the outgoing channel, relativistic three-body kinematics are fully taken into account. Projectile-target interactions are described in a folding model using the NN T-matrix at 1 GeV of Franey and Love [34].

In order to investigate the sensitivity of the removal process to binding energies, the calculations were performed for several one-neutron separation energies, $S_n = 160$, 260, and 500 keV. In table 4 the dependence of the theoretical removal cross-sections and momentum widths on the separation energy is displayed for the carbon target. The lowest value, $S_n = 160$ keV, can be ruled out because it leads to a too narrow momentum distribution, while the one-neutron removal cross-section is still within the experimental uncertainty. The calculations indicate a clear preference for a larger separation energy. Good agreement with the data is found for $S_n = 260$ keV, but slightly larger values would still lead to an acceptable description of the data where $S_n = 500$ keV seems to constitute an upper limit.

Breakup calculations for ^{19}C on a ^{208}Pb target at $E_{lab} = 910$ MeV/u also indicate a preference for a neutron separation energy being larger than 260 keV but smaller than 500 keV. For the lead target, the calculations predict a strong dependence of the removal cross-section on the separation energy, changing from $\sigma_{-1n} = 2778$ mb for $S_n = 260$ keV to $\sigma_{-1n} = 1180$ mb for $S_n = 500$ keV. These values have to be compared to the measured value of $\sigma^{exp}_{-1n} = 1967 \pm 334$ mb (see table 3). A systematic search shows that the experimental removal cross-section is reproduced within the error for 315 keV$< S_n <$ 433 keV, with a mean value of $S_n = 364$ keV. For the carbon target σ_{-1n} is found to depend only weakly on a variation of S_n over the chosen range (*e.g.* the calculation for $S_n = 364$ keV leads to $\sigma_{-1n} = 191$ mb, very close to the value obtained for $S_n = 260$ keV).

For ^{17}C, the DCP calculations predict a $5/2^+$ ground state with a neutron separation energy of $S_n = 715$ keV. The ^{16}C(0^+, g.s.) $\otimes 1d_{5/2}$ mean-field configuration carries a spectroscopic factor of 0.61. Hence, configuration mixing is also significant for this nucleus, accounting for the remaining 39% of the valence wave function. Among the core-excited configurations the coupling of $d_{5/2}, s_{1/2}$, and

[1] The spectroscopic factors are normalized to the BCS occupation probabilities.

$d_{3/2}$ single particle states to the first excited 2^+ state, ^{16}C (2^+_1,1.76), are the most important ones. The largest contribution with a spectroscopic factor of 0.25 is due to $^{16}\mathrm{C}(2^+_1)\otimes 1d_{5/2}$. $J^\pi = 1/2^+$ states couple to the 2^+_1 state over a wide range of mean-field orbitals resulting in a summed total spectroscopic strength of 0.10. For $^{16}\mathrm{C}(2^+_1)\otimes d_{3/2}$ a total contribution of 0.03 is obtained. Interestingly, about half of $^{16}\mathrm{C}(2^+_1)\otimes 1/2^+$ and all of the $3/2^+$ strength originate from unbound mean-field orbitals. Hence, the importance of the coupling to the continuum in dripline nuclei is already observable in ^{17}C. A good agreement between our data and the DCP calculation is found for a ^{17}C ground state of $5/2^+$ (table 5). However, we do not want to ignore recent results obtained at MSU for ^{17}C breakup [29]. This work allows to assign a spin and parity of $3/2^+$ for the ^{17}C ground state from the analysis of the coincidences between γ-rays and knock-out fragments, and the authors conclude that the most important contributions to the ^{17}C ground state involve single-particle orbitals coupled to $^{16}\mathrm{C}(2^+_1)$.

Our breakup calculations for ^{17,19}C indicate strong contributions from final-state interactions (FSI) between the ejected neutron and the core nucleus. Without FSI the ^{19}C removal cross-section and momentum width are reduced by about 20%. The structure calculations predict a large number of low-lying "bound states embedded in the continuum" (BSEC) [35,36] for ^{17,19}C, leading to a delayed emission of the knockout particle through interactions with core-excited configurations. The BSEC are given by quasi-bound core-excited configurations with total energy above the particle threshold, but decaying only through the coupling to the asymptotically open single-particle continuum states. In ^{17,19}C, the formation of BSEC is especially favored by the density of continuum s-states and d-wave resonances close to the threshold. In populating these states, the knocked-out neutron remains strongly correlated to the core after the breakup process. Interestingly, this feature seems to be characteristic for the odd-mass carbon isotopes. A confirmed case is the $3/2^+$ continuum state in ^{13}C, which was predicted by Baur and Lenske [35] and measured in an $(\alpha,\alpha'\mathrm{n})$ reaction [36]. The present, more elaborate calculations predict a strong enhancement of BSEC formation for the carbon isotopes with increasing neutron excess.

In table 5, theoretical results for removal cross-sections together with the widths of the momentum distributions after one-neutron removal are listed. The widths Γ_p (FWHM) of the longitudinal momentum distributions after one-neutron removal reported by Baumann *et al.* [18, 26] are included for comparison. The theoretical results reported for ^{19}C in table 5 were obtained with $S_\mathrm{n} = 260$ keV. In general, the calculations show a close correspondence between the magnitude of the removal cross-sections and the spectroscopic properties of the removed nucleon. Of particular interest is the close relationship to the longitudinal momentum distribution. For example, the measured ^{18}C momentum distribution from ^{19}C breakup can in principle also be reproduced by assuming a strongly mixed $5/2^+$ or $3/2^+$ ground state with a large content of core-excited $2s_{1/2}$ strength. Compared to experimental data, however, the corresponding removal cross-section is too low by about a factor of 4.

4 Conclusions

We measured one-nucleon removal cross-sections for a variety of boron and carbon isotopes. We compare results for ^{8}B and ^{19}C, which are of special interest because of their halo character, to those of stable boron and carbon nuclei. We observe a correlation of the magnitude of the removal cross-sections with the widths of the longitudinal momentum distributions in approaching either the neutron or proton dripline. The measurements show that removal cross-sections provide important nuclear structure information complementary to that obtained from momentum distributions of breakup fragments.

The combination of these results with the small widths of the momentum distributions for the corresponding fragments (see also refs. [17,18]) lends independent support for the existence of a 1n-halo structure in ^{19}C and a 1p-halo in ^{8}B. This allows to constrain assignments of ground-state spins and parities. A good example is ^{19}C, where the combined analysis of one-nucleon removal cross-section and longitudinal momentum distribution clearly requires a $J^\pi = 1/2^+$ ground state. In addition, the analysis of the ^{19}C one-neutron removal cross-section on a lead target gave evidence for a neutron separation energy around $S_\mathrm{n} = 330$ keV, close to the value of $S_\mathrm{n} = 530 \pm 130$ keV obtained by Nakamura *et al.* [3].

This work was partially supported by Deutsche Forschungsgemeinschaft (DFG) under contract Le403/4, by Bundesministerium für Bildung, Wissenschaft, Forschung und Technologie (BMBF) under contract DA820, and by Internationales Büro Osteuropa-Verbindungsbüro des BMBF bei dem DLR under contract WTZ Bonn SLA-002-96.

References

1. G. Audi et al., Nucl. Phys. A **595**, 409 (1995).
2. F.M. Marqués et al., Phys. Lett. B **381**, 407 (1996).
3. T. Nakamura et al., Phys. Rev. Lett. **83** 1112 (1999).
4. I. Tanihata et al., Phys. Rev. Lett. **55** 2676 (1985).
5. F. Negoita et al., Phys . Rev. C **54**, 1787 (1996).
6. R.E. Warner et al., Phys. Rev. C **52**, R1166 (1995).
7. R.E. Warner et al., Phys. Rev. C **54**, 1700 (1996).
8. M.M Obuti et al., Nucl. Phys. A **609**, 74 (1996).
9. M. Fukuda et al., Nucl. Phys. A **656**, 209 (1999).
10. I. Tanihata et al., Phys. Lett. B **206**, 592 (1988).
11. W. Schwab et al., Z. Phys. A **350**, 283 (1995).
12. B. Blank et al., Nucl. Phys. A **624**, 242 (1997).
13. A. Ozawa et al., to be published in Nucl. Phys. A.
14. J.H. Kelly et al., Phys. Rev. Lett. **74**, 30 (1995).
15. D. Bazin et al., Phys. Rev. Lett. **74**, 3569 (1995).
16. D. Bazin et al., Phys. Rev. C **57**, 2156 (1998).
17. M.H. Smedberg et al., Phys. Lett. B **452**, 1 (1999).
18. T. Baumann et al., Phys. Lett. B **439**, 256 (1998).

19. D.L. Olson et al., Phys. Rev. C **28**, 1602 (1983).
20. H. Geissel et al., Nucl. Instrum. Methods B **70**, 286 (1992).
21. N. Iwasa et al., Nucl. Instrum. Methods B **126**, 284 (1997).
22. S. Fortier et al., Phys. Lett. B **461**, 22 (1999).
23. T. Aumann et al., Phys. Rev. Lett. **84**, 34 (2000).
24. H. Lenske, J. Phys. G **24**, 1429 (1998).
25. R. Shyam, H. Lenske, Phys. Rev. C **57**, 2427 (1998).
26. T. Baumann, Ph.D. thesis, Universität Giessen (1999).
27. D. Ridikas, M.H. Smedberg, J.S Vaagen, M.V. Zhukov, Nucl. Phys. A **628**, 363 (1998).
28. J.A. Tostevin, J.S. Al-Khalili, Phys. Rev. C **59**, R5 (1999).
29. V. Maddalena et al., Preprint MSUCL-1171 August(2000).
30. F.J. Eckle et al., Phys. Rev. C **39**, 1662 (1989).
31. F.J. Eckle et al., Nucl. Phys. A **506**, 199 (1990).
32. H. Lenske, in preparation.
33. N. Vinh Mau, Nucl. Phys. A **592**, 33 (1995).
34. M.A. Franey, W.G. Love, Phys. Rev. C **31**, 488 (1985).
35. G. Baur, H. Lenske, Nucl. Phys. A **282**, 201 (1977).
36. H. Fuchs et al., Nucl. Phys. A **343**, 133 (1980).